Journal of Digital Imaging (2020) 33:221–230
https://doi.org/10.1007/s10278-019-00223-1

Fully Automated Lung Lobe Segmentation in Volumetric Chest CT with 3D U-Net: Validation with Intra- and Extra-Datasets

Jongha Park[1] · Jihye Yun[1] · Namkug Kim[1] · Beomhee Park[1] · Yongwon Cho[1] · Hee Jun Park[1] · Mijeong Song[1] · Minho Lee[2] · Joon Beom Seo[3]

Published online: 31 May 2019

Abstract

Lung lobe segmentation in chest CT has been used for the analysis of lung functions and surgical planning. However, accurate lobe segmentation is difficult as 80% of patients have incomplete and/or fake fissures. Furthermore, lung diseases such as chronic obstructive pulmonary disease (COPD) can increase the difficulty of differentiating the lobar fissures. Lobar fissures have similar intensities to those of the vessels and airway wall, which could lead to segmentation error in automated segmentation. In this study, a fully automated lung lobe segmentation method with 3D U-Net was developed and validated with internal and external datasets. The volumetric chest CT scans of 196 normal and mild-to-moderate COPD patients from three centers were obtained. Each scan was segmented using a conventional image processing method and manually corrected by an expert thoracic radiologist to create gold standards. The lobe regions in the CT images were then segmented using a 3D U-Net architecture with a deep convolutional neural network (CNN) using separate training, validation, and test datasets. In addition, 40 independent external CT images were used to evaluate the model. The segmentation results for both the conventional and deep learning methods were compared quantitatively to the gold standards using four accuracy metrics including the Dice similarity coefficient (DSC), Jaccard similarity coefficient (JSC), mean surface distance (MSD), and Hausdorff surface distance (HSD). In internal validation, the segmentation method achieved high accuracy for the DSC, JSC, MSD, and HSD (0.97 ± 0.02, 0.94 ± 0.03, 0.69 ± 0.36, and 17.12 ± 11.07, respectively). In external validation, high accuracy was also obtained for the DSC, JSC, MSD, and HSD (0.96 ± 0.02, 0.92 ± 0.04, 1.31 ± 0.56, and 27.89 ± 7.50, respectively). This method took 6.49 ± 1.19 s and 8.61 ± 1.08 s for lobe segmentation of the left and right lungs, respectively. Although various automatic lung lobe segmentation methods have been developed, it is difficult to develop a robust segmentation method. However, the deep learning–based 3D U-Net method showed reasonable segmentation accuracy and computational time. In addition, this method could be adapted and applied to severe lung diseases in a clinical workflow.

Keywords 3D U-net · Convolutional neural network · Deep learning · Lung lobe segmentation

Introduction

The human lungs are anatomically and functionally divided into five distinct compartments called lobes, which are separated by the lobar fissures. As the airway and vessel tree system are independently distributed in each lobe, many lung diseases preferentially affect a particular lobar level [1]. Emphysema, post-primary tuberculosis, and silicosis typically affect the upper lobes, whereas idiopathic pulmonary fibrosis is commonly associated with the lower lobes [2–5]. In addition, treatment options including lung cancer surgery and lung volume reduction surgery are performed at a lobar level. Therefore, lung lobe segmentation in volumetric chest computed tomography (CT) plays an important role in measuring

Jongha Park and Jihye Yun contributed equally to this work

✉ Namkug Kim
namkugkim@gmail.com

[1] Department of Convergence Medicine, University of Ulsan College of Medicine, Asan Medical Center, 388-1 Pungnap2-dong, Songpa-gu, Seoul, Republic of Korea

[2] Biomedical Research Institute & Department of Radiology, Seoul National University Hospital (SNUH), 101, Daehak-ro Jongno-gu, Seoul 03080, Republic of Korea

[3] Department of Radiology, University of Ulsan College of Medicine, Asan Medical Center, 388-1 Pungnap2-dong, Songpa-gu Seoul, Republic of Korea

Table 1 Configurations of multi-center chest CT scans at inspiration and expiration

Chest CT dataset	Training	Validation	Test (internal dataset)	Test (external dataset)	Total
Asan Medical Center	172	24	20	–	216
Kangbuk Samsung Hospital	100	16	20	–	136
Konkuk University Hospital	–	–	–	40	40
Total	272	40	40	40	392

lung functions and regional image analysis including texture and shape analyses at a lobar level and surgical planning. Manual lobe segmentation is too time-consuming and involves some degree of inter-observer variability; thus, fully automated lung lobe segmentation is needed. The lobar fissures, which are the basis for lobe segmentation, have similar intensities to those of their neighboring structures such as pulmonary vessels and are anatomically different between individuals; fissures are often incomplete or absent and can vary greatly in shape and location, especially in the presence of a disease (e.g., infiltrative lung disease). These characteristics could lead to segmentation error in automated segmentation methods.

Various automatic approaches have been proposed for lung lobe segmentation. Lassen et al. proposed a method based on Hessian analysis to model sheet-like, tubular, and blob-like structures by the eigenvalues of the Hessian matrix, which is a matrix built of the second partial derivatives of an image [6, 7]. This method worked well in normal cases but was sensitive to CT scan protocols/parameters, image noise, and incompleteness of fissures; in particular, it did not work in the case of chronic obstructive pulmonary disease (COPD). Zhang et al. presented an atlas-based method that trains the structural shapes based on existing gold standards [8]. This method achieved good results but was time-consuming and it showed a relatively poorer performance when the disease changed the structures of the lungs. There are other segmentation methods based on thresholding, surface fitting [9], watersheding [10], and graph searching with shape constraints [11]. However, these methods need parameter optimization (e.g., smoothness and thresholding values) for the best performance because they are vulnerable to the image quality level. In addition, intensity-based methods are challenging due to the similar intensity to those of image noise, vessels, airway walls, and other structures. Therefore, these fully automated segmentation methods could not be used in clinical applications.

Recently, deep learning architectures have been successfully established for lung lobe segmentation. George et al. used a progressive, holistically nested network [12] to segment lobar boundaries, generating seed points and edge probabilities for a random walker, which could produce a final lobe segmentation mask [13]. This method showed good results not only for the normal group but also for the COPD group. However, it relied on prior segmentation of the lobar boundaries (i.e., fissures) and thus did not work well for lungs with fake or incomplete fissures.

In this study, we performed lung lobe segmentation using a deep learning technique to develop a robust algorithm without lobar fissure detection. We applied a 3D convolutional neural network (CNN) to exploit the geometric information of the lungs. Our method outperformed image processing–based segmentation in terms of accuracy and execution time. Validation with internal and external datasets demonstrated that our fully automated segmentation method could be applied to clinical radiology.

Table 2 Basic conditions for each localized structure

λ_1	λ_2	λ_3	Structure orientation
L	L	L	Noise (no preferred structure)
L	L	H−	Bright sheet-like structure
L	L	H+	Dark sheet-like structure
L	H−	H−	Bright tubular structure
L	H+	H+	Dark tubular structure
H−	H−	H−	Bright blob-like structure
H+	H+	H+	Dark blob-like structure

$|\lambda_1| \le |\lambda_2| \le |\lambda_3|$ are eigenvalues of Hessian matrix, L: $\lambda_i \cong 0$, H+: λ_i is high positive value, H−: λ_i is high negative value

Materials and Methods

Patient Datasets

For algorithm development, we obtained the chest CT scans of mild-to-moderate COPD patients at full inspiration and expiration, which included three different datasets from Kangbuk Samsung Hospital (68 patients), Asan Medical Center (108 patients), and Konkuk University Hospital (20 patients) in South Korea. These multi-center datasets were composed of independent heterogeneous sets with different scanners, reconstruction kernels, and severities of COPD: (1) Asan Medical Center—a 16-channel multi-detector CT (MDCT) scanner (Somatom Sensation 16; Siemens Healthcare, Erlangen, Germany) with 140 kVp, 100 eff. mA/s, a slice thickness of 0.75 mm, and a reconstruction kernel of B30f; (2) Kangbuk Samsung Hospital—a 40-channel MDCT scanner (Brilliance 40; Philips Healthcare, Best, The Netherlands)

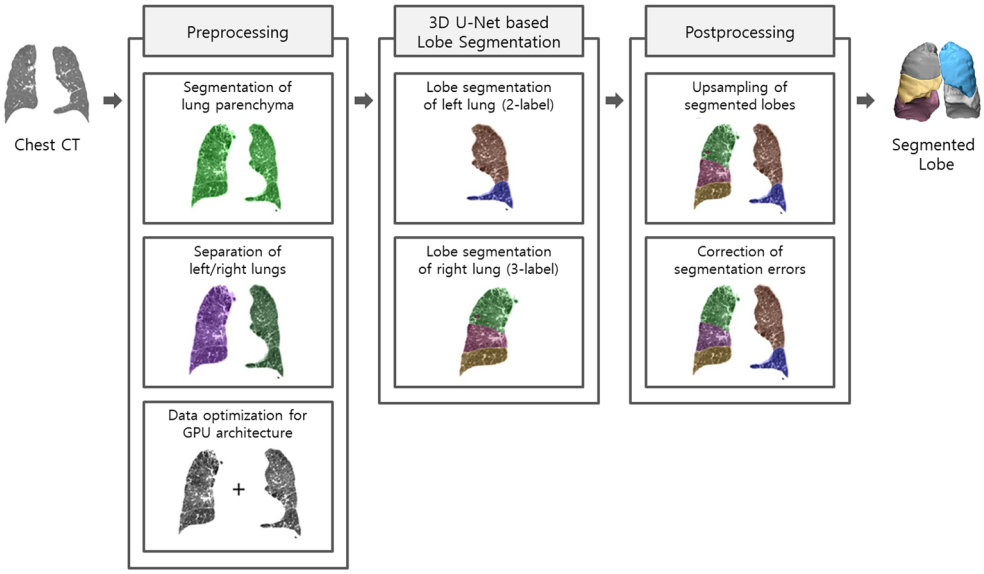

Fig. 1 Overall process of the proposed lung lobe segmentation method

with 140 kVp, 110 mA/s, a slice thickness of 0.8 mm, and a reconstruction kernel of B; (3) Konkuk University Hospital—a 64-channel MDCT scanner (Brilliance 64; Philips Healthcare, Best, The Netherlands) with 140 kVp, 183 mA/s, a slice thickness of 0.625 mm, and a reconstruction kernel of B. These datasets were split into training (272 CT scans), validation (40 scans), and test (40 scans) datasets. The CT scans of Konkuk University Hospital were used only for external validation (see Table 1).

Gold Standard of Lung Lobe Segmentation

Since manual lobe segmentation is too time-consuming and difficult, we semi-automatically segmented all images based on Hessian analysis [6], which was previously developed. The Hessian analysis is a segmentation technique based on the Hessian matrix which is derived from the second derivatives:

$$H(\mathrm{x},\mathrm{y},\mathrm{z}) = \nabla^2 \begin{bmatrix} f_{xx} & f_{xy} & f_{xz} \\ f_{yx} & f_{yy} & f_{yz} \\ f_{zx} & f_{zy} & f_{zz} \end{bmatrix} \quad (1)$$

The eigenvalues ($|\lambda_1| \le |\lambda_2| \le |\lambda_3|$) of the Hessian matrix characterize the local morphological structure of an object, such as sheet-like, tubular, and blob-like structures [6] (see Table 2). The lobar fissures were segmented using the conditions of sheet-like structures. To characterize the structures of interest, suppress local noises and perform Hessian analysis in CT images, we used Gaussian smoothing with $\mathbf{3} \times \mathbf{3} \times \mathbf{3}$ kernel convolution before $\mathbf{3} \times \mathbf{3} \times \mathbf{3}$ Hessian analysis with 1-pixel stride moving window. These segmented lobe regions were confirmed and modified by expert radiographers with more than 5 years of experience using the in-house software AView, which included several modules of lung segmentation, left/right lung separation, Hessian analysis–based lobe segmentation, and manual editing tools.

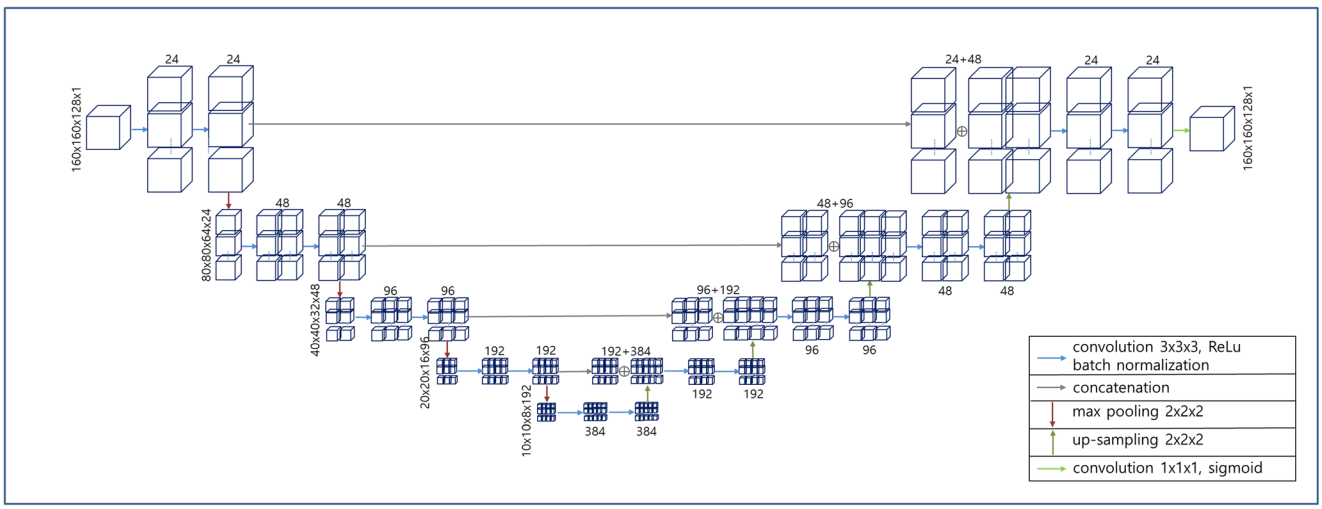

Fig. 2 Architecture of 3D U-Net

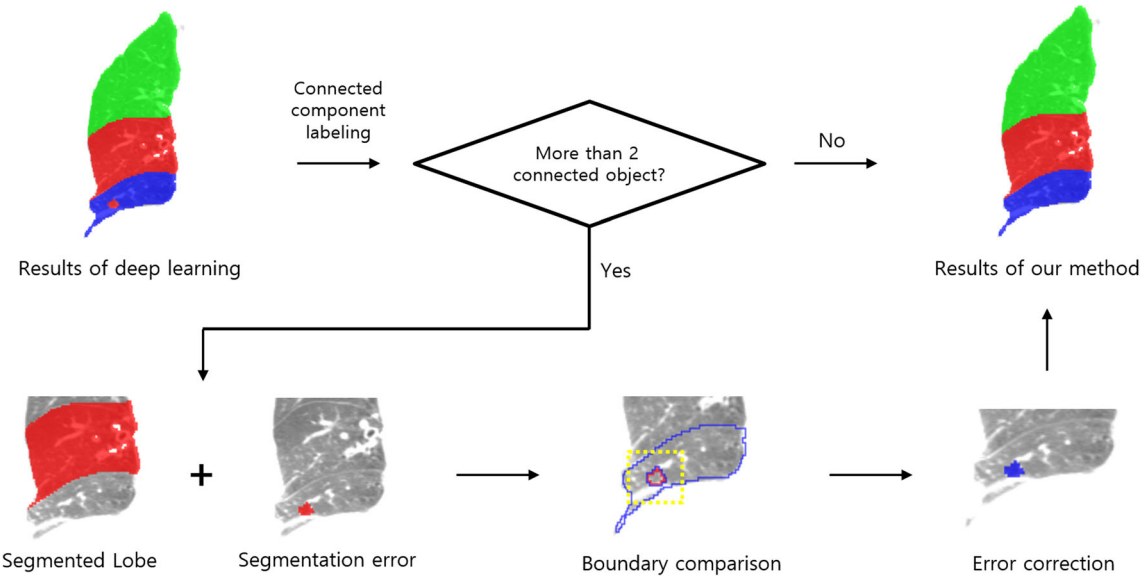

Fig. 3 Process of segmentation error correction

Fully Automated Lung Lobe Segmentation Using 3D U-Net

Lung lobe segmentation would likely be better performed by 3D CNN, since lung lobes are 3D objects, and 2D CNN do not consider 3D continuity between slices, which guarantees 3D continuity of segmented lobes. In addition, since it is frequently found that human lungs have incomplete and/or fake fissures [14], fissure-based lung lobe segmentation could be susceptible to these anatomical variations. We, therefore, introduced 3D CNN to fully automated 3D lung lobe segmentation without lobar fissure detection. Our system proceeds through three main steps (Fig. 1). To segment the left and right lung lobes with different geometric structures, we split whole lungs into the left and right lungs and optimize them for GPU architectures. From each of left and right lungs, the lobes are segmented using 3D U-Net. Finally, the segmentation errors are corrected by boundary comparison.

Preprocessing

The geometric structures of the left and right lungs are different (not symmetrical) as the left lung has two lobes but the right lung has three. Our method trained these different left and right lungs separately. First, we segmented the lungs by thresholding (ranging from − 1024 HU to − 400 HU) and using region-growing techniques [15]. To handle the hilar regions, the airways were excluded by thresholding (ranging from − 1024 HU to − 950 HU) and region growing with an initial seed point, which was automatically detected by the circle detection algorithm. As the airways have circle-like shapes in the axial plane, they could be excluded by the modified Hough transform [16], which was performed on the upper slices (5%) based on the z-axis. Second, the segmented lungs were split into the left and right lungs. When the left and right lungs were weakly connected, they were easily separated using a small number of iterations based on 3D morphological operations, 3D distance transform, and surface fitting algorithms [17, 18]. To check if the lungs are

Table 3 Definitions of evaluation metrics

Evaluation metric	Definition	
DSC (X, Y)	$\frac{2\lvert X\cap Y\rvert}{\lvert X\rvert+\lvert Y\rvert}$	[2]
JSC (X, Y)	$\frac{\lvert X\cap Y\rvert}{\lvert X\cup Y\rvert}$	[3]
MSD (X, Y)	$\frac{1}{N_X+N_Y}\left\{\sum_{x\in S_X}\min_{y\in S_Y}(\mathrm{dist}(x,y))+\sum_{y\in S_Y}\min_{x\in S_X}(\mathrm{dist}(x,y))\right\}$	[4]
HSD (X, Y)	$\max\left\{\sup_{x\in S_X}\inf_{y\in S_Y}\mathrm{dist}(x,y),\sup_{y\in S_Y}\inf_{x\in S_X}\mathrm{dist}(x,y)\right\}$	[5]

Optimal value of DSC, JSC, MSD, and HSD was 1, 1, 0, and 0, respectively

Table 4 Performance of the proposed lung lobe segmentation method evaluated with the internal-dataset

$N = 40$	LtLower	LtUpper	RtLower	RtMiddle	RtUpper	Overall
DSC	0.9721 ± 0.011	0.9806 ± 0.007	0.9684 ± 0.012	0.9436 ± 0.019	0.9753 ± 0.012	0.9680 ± 0.018
JSC	0.9460 ± 0.021	0.9620 ± 0.014	0.9389 ± 0.022	0.8938 ± 0.033	0.9520 ± 0.022	0.9385 ± 0.031
MSD (mm)	0.5796 ± 0.240	0.5092 ± 0.231	0.6901 ± 0.246	1.0239 ± 0.415	0.6545 ± 0.413	0.6914 ± 0.364
HSD (mm)	14.40 ± 5.85	18.20 ± 12.06	17.59 ± 13.68	18.55 ± 8.47	16.86 ± 13.24	17.12 ± 11.07

Lt, left; *Rt*, right

separated, connected component labeling [19] were used. At this stage, if only one connected object was detected, we judged this lung has strongly connected, the next step was performed. When the left and right lungs were strongly connected, the junction parts between them were weakened by morphological operation and Hessian analysis. In a similar manner as in the generation of the gold standard, the junction parts were detected and excluded using a combination of eigenvalues for sheet-like structures. Finally, the separated left/right lungs were resized to 160×160×128 in order to optimize the data for GPU architectures. In our method, lung segmentation and half-lung separation of our previous study were performed to obtain rough coordinates and size of square-cropped each lung image [17].

Generalized Segmentation Using 3D U-Net

In order to capture the 3D information of the lobar fissures, we applied 3D U-Net [20], which extended the U-Net architecture from Ronneberger et al. [21] by replacing all 2D operations with their 3D counterparts. U-Net, which is a type of fully convolutional network [22], is one of the most widely used CNN architectures for image segmentation. 3D U-Net consists of the analysis and synthesis paths, and each path has four resolution layers (Fig. 2). In the analysis path, each layer is composed of two steps of 3×3×3 convolution followed by a rectified linear unit (ReLU) as well as 2×2×2 max pooling with strides of two in each dimension, which can reduce dimensions. In the synthesis path, each layer is composed of an up-convolution of 2×2×2 by strides of two in each dimension as well as two 3×3×3 convolutions followed by a ReLU, which can extend dimensions. One of the advantages of 3D U-Net is the concatenation of layers of equal resolution, preventing loss of information at the deeper layers.

We applied the 3D U-Net architecture to lung lobe segmentation with the structural hyper-parameters including an input size of 160×160×128, since the size of input images needs to be unified for training. Our 3D U-Net was implemented in Keras using Theano, and we used cuDNN convolution layers for efficient memory management. Given the training datasets (272 cases for training and 40 cases for validation), our 3D U-Net was learned by minimizing the training error, i.e., the Dice similarity coefficient [23] (DSC) between the inferred label and the gold standard label. The training error was minimized by running the back-propagation algorithm and it took around 3 days using TITAN XP with 12 GB GPU. With separately trained optimal models for the left and right lungs, we then segmented the lung lobes. The final lung lobes were obtained by upsampling and correction of segmentation error. Since each lung lobe is a single continuous object, we defined that they included the segmentation error in case of the segmentation results having more than two objects. These problems sometimes happened, and we detected the segmentation errors using connected component labeling, and then these errors were corrected by boundary comparison (Fig. 3).

Evaluation Metric and Statistical Analysis

In this study, three methods including Hessian analysis–based segmentation [6] with manual correction, semi-automatic segmentation with manual correction using the in-house software

Table 5 Comparison of the performance and execution time of different methods

$N = 5$	Hessian analysis–based segmentation (with manual correction)	Grid-fitting-based segmentation (with manual correction)	Our method (fully automated)
Left lung (s)	220.12 ± 66.20	83.00 ± 13.87	6.49 ± 1.19
Right lung (s)	357.22 ± 90.02	200.60 ± 43.75	8.61 ± 1.08
Accuracy (overall DSC)	0.915 ± 0.10	0.962 ± 0.022	0.948 ± 0.018
Accuracy (overall JSC)	0.857 ± 0.150	0.928 ± 0.040	0.901 ± 0.032
Accuracy (overall MSD)	2.48 ± 3.22	0.90 ± 0.46	1.36 ± 0.75
Accuracy (overall HSD)	45.23 ± 28.80	21.82 ± 7.31	28.93 ± 14.24

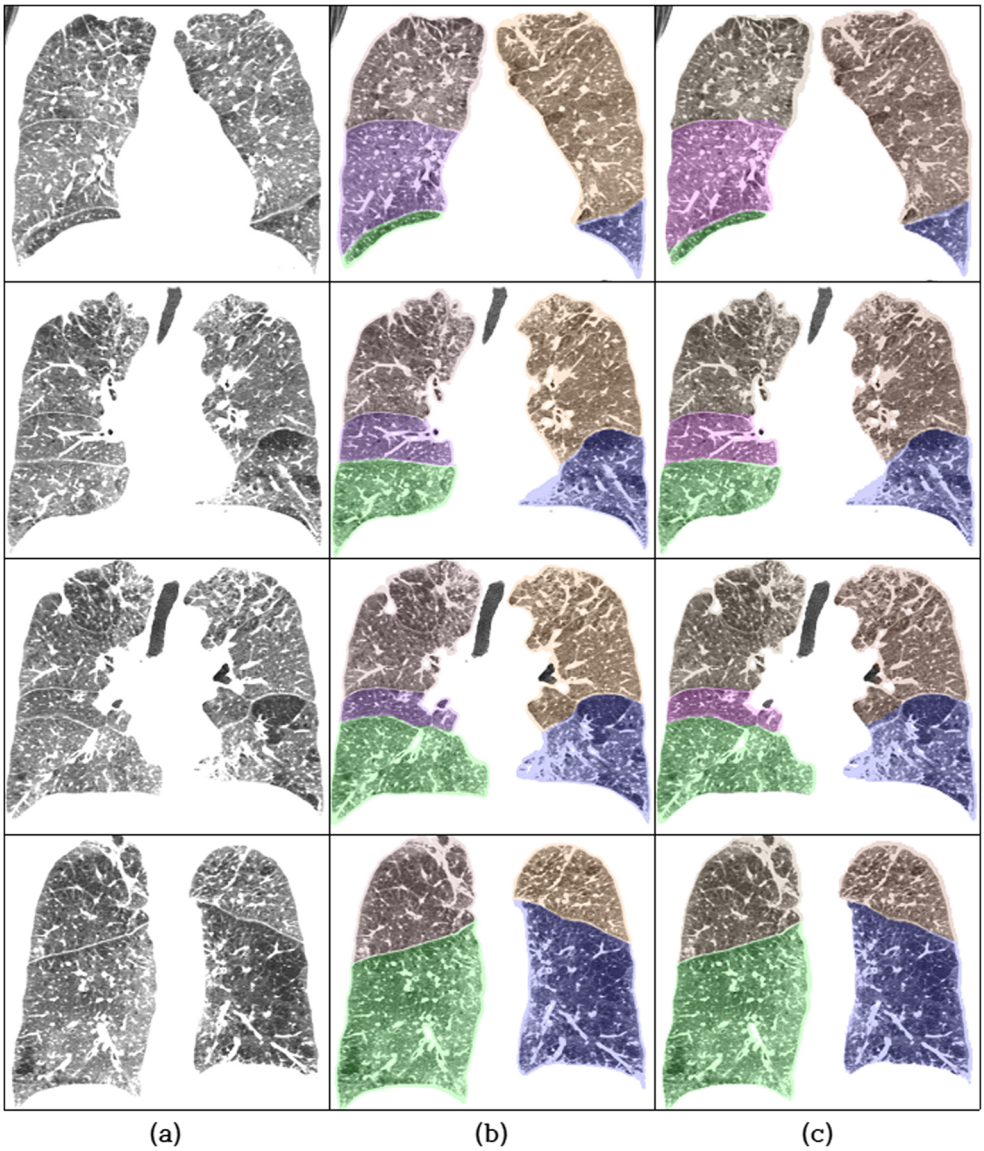

Fig. 4 Result images of the external validation. Rows from upper to lower show coronal images with segmentation results from anterior to posterior of a patient CT scan. **a** Chest CT scans. **b** Gold standard. **c** Segmentation results

AView, and our proposed method were compared in terms of segmentation accuracy and processing time. All of the three methods assumed that the lung segmentation and separation of the left and right lungs are complete. Hessian analysis–based segmentation requires user interaction as it is highly sensitive to parameter settings and contains false positives. In the case of semi-automatic segmentation, we used a grid-fitting algorithm [24] including a manual drawing of fissures and corrections.

The performance of the proposed method was evaluated with two types of independent datasets: internal and external datasets. Each segmentation result was evaluated and compared with the gold standard. To quantify the comparisons, we computed the DSC and Jaccard similarity coefficient [25] (JSC). In addition, the mean surface distance (MSD) and Hausdorff surface distance [26] (HSD) were also computed as the DSC and JSC are presented as a high value in the case of large objects. Our evaluation metrics are defined in Table 3. $|X|$ is the number of voxels in volume X, and S_X is the surface (i.e., border voxels) of X. N_X is the number of voxels on S_X, and dist(x, y) is the voxel distance between x and y.

Results

Internal Validation of Lung Lobe Segmentation

The analysis of our datasets was challenging as they were derived from mild-to-moderate COPD patients. Table 4 summarizes the performance of all four metrics (DSC, JSC, MSD, and HSD) with the internal dataset (40 cases not used for training). The overall DSC, JSC, MSD, and HSD were 0.9680 ± 0.018, 0.9385 ± 0.031, 0.6914 ± 0.364, and 17.12 ± 11.07, respectively. Although the segmentation of the right middle lobe is usually difficult, we obtained good

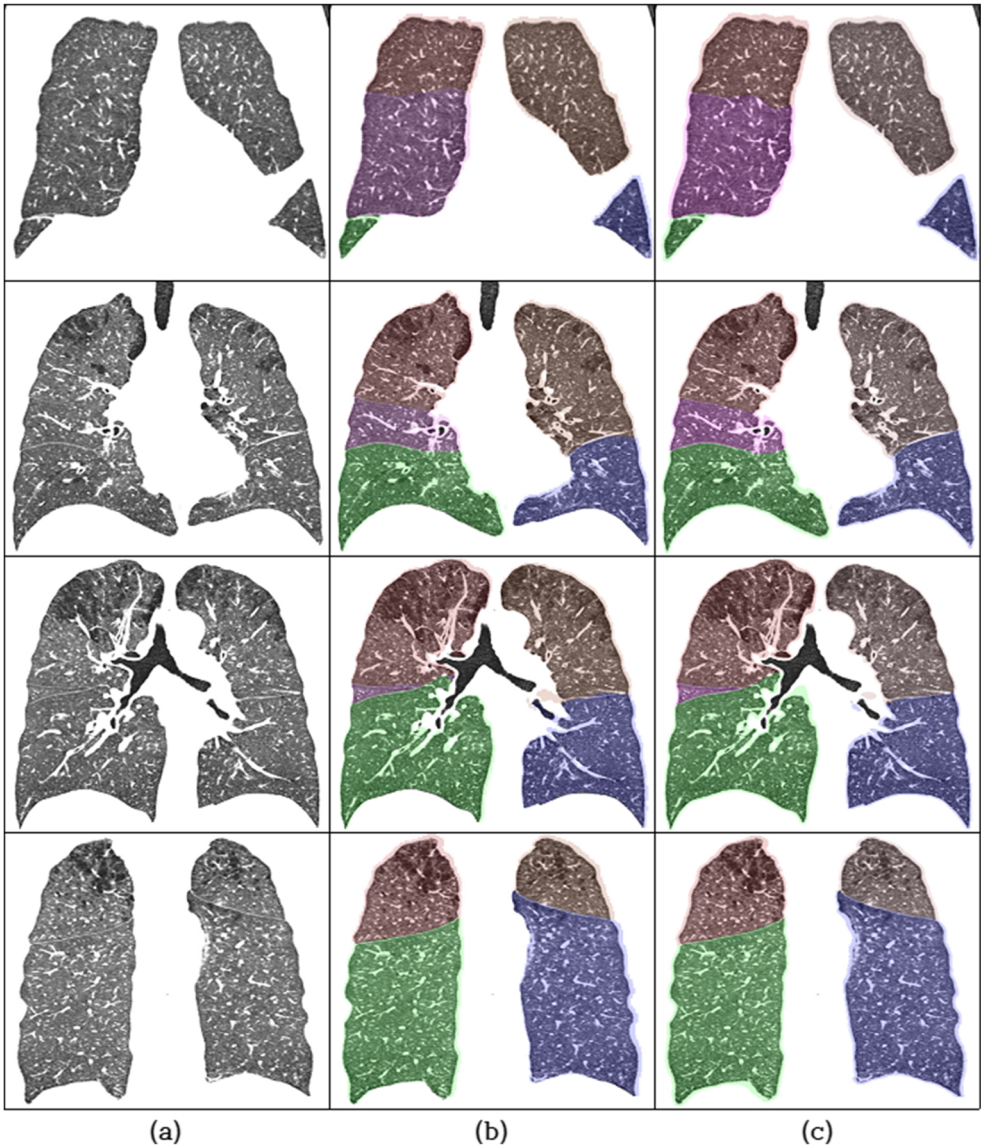

Fig. 5 Result images of external validation in case of incomplete fissures. Rows from upper to lower show coronal images with segmentation results from anterior to posterior of a patient CT scan. **a** Chest CT scans. **b** Gold standards. **c** Segmentation results

results with a DSC of 0.9436 ± 0.019 and JSC of 0.8938 ± 0.033. Table 5 shows a comparison of the average execution time of three methods including Hessian analysis–based segmentation with manual correction, semi-automatic segmentation with manual correction using the in-house software AView, and our proposed method. The Hessian analysis–based segmentation and semi-automatic segmentation methods required manual corrections or interactions; thus, the execution time was long. Although our method could be used with a large number of datasets, we used only five cases for comparison with other methods; these five cases were randomly selected from the internal datasets. These experiments were performed for comparing execution time of each method without algorithms failure. Our fully automated

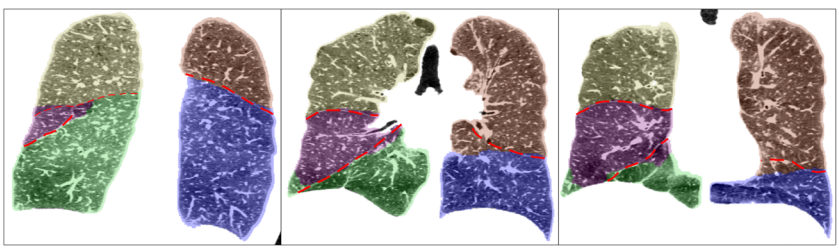

Fig. 6 Segmentation results of coronal images of a poor case with fissures of the gold standard (red dashed lines) from anterior to posterior (left to right images). Quantification results including DSC, JSC, MSD, and HSD were 0.9445, 0.8954, 1.698, and 31.482, respectively

method required an average of 6.49 ± 1.19 s for the left lobes and 8.61 ± 1.08 s for the right lobes on Intel Xeon E5-2620 v3 @ 2.4 GHz, 6-core CPU, 32 GB RAM, GeForce GTX 1080 with 8 GB, and Windows 10 OS. Figures 4 and 5 show that our method was robust even in cases with incomplete fissures, while Fig. 6 shows the case of poor performance.

External Validation of Lung Lobe Segmentation

In order to evaluate the generalizability of our model, we performed an external validation using an independent dataset with the training step. The external dataset was from Konkuk University Hospital, which was scanned with a different scanner and reconstruction kernel. Table 6 summarizes the performance of the external validation with all four metrics (DSC, JSC, MSD, and HSD). Although this dataset was substantially different from the training dataset, our method achieved a high accuracy with a DSC of 0.96 ± 0.02, JSC of 0.92 ± 0.03, MSD of 1.31 ± 0.56, and HSD of 27.89 ± 7.50. Especially for the right middle lobe, which is a very challenging task for segmentation that shows a reasonable accuracy with a DSC of 0.93 ± 0.03, JSC of 0.87 ± 0.05, MSD of 1.48 ± 0.84, and HSD of 23.29 ± 8.94. In general, our method shows a robust performance on all test cases with higher accuracies with small standard deviations. Furthermore, we evaluated the performance of our method according to COPD severity based on COPD GOLD guidelines [27]. The higher COPD GOLD stage means more severe COPD. Table 7 shows good and similar results regardless of COPD severity.

Discussion

Previously proposed automatic techniques for lung lobe segmentation are sensitive to anatomic and disease variations, reconstruction kernels, and parameter settings, making it impossible to fully automate the segmentation of the data. These techniques could be used only for the initial segmentation with manual correction and parameter settings. 3D lung lobe segmentation is costly, time-consuming, and laborious; it frequently requires manual correction by expert radiologists, which is a barrier to application in a clinical workflow. To overcome these problems, we proposed a fully automated lung lobe segmentation method, which could produce high-quality results without manual correction. George et al. [12] proposed another method of lung lobe segmentation using progressive holistically nested networks and the random walker algorithm. The method in this study also demonstrated good results for the normal group and the COPD group. However, similar to most other methods, it relied on prior segmentation of the lobar fissures, which had problems with fake or incomplete fissures. Fake fissures could generate segmentation error and negatively affect the segmentation result. In addition, the method would not work in the case of incomplete fissures. Some automatic algorithms produce less accurate results because they could not distinguish minor fissures on the right lung. To address these problems, we trained the lung lobe without lobar fissure information (Fig. 6).

Parameter optimization of the conventional methods for lung lobe segmentation is very sensitive to disease severity. The evaluation of our method according to the COPD GOLD stage demonstrated the robustness of our method to disease variation.

In this study, there are several limitations. We selected mild-to-moderate COPD patients in this study. However, when a lung disease becomes severe, the lung structures would change considerably. For a more robust clinical outcome, patients with strong anatomical variations, various lung diseases including severe COPD with emphysema, diffuse infiltrative lung disease (DILD) with complex parenchymal texture patterns, post-primary tuberculosis, and cancer which could have potentials to change pathological lung and lobe anatomy should be included. In addition, quality of lung segmentation could affect that of lobe segmentation, especially in DILD patients, which could be enhanced by developing deep learning method for lung segmentation. In future studies, we will evaluate the performance of this method using open dataset on lung lobe segmentation and develop a more robust lung segmentation method based on this method using more high-quality segmentation labels. In addition, we may build larger datasets for lung lobe segmentation, which could lead to the development of another robust lobe segmentation method. To build larger datasets, we could develop an easy user interface, fast processing, initial segmentation techniques, and correction modules.

Table 6 Performance of the proposed lung lobe segmentation method evaluated with the external dataset

N = 40	LtLower	LtUpper	RtLower	RtMiddle	RtUpper	Overall
DSC	0.9556 ± 0.013	0.9701 ± 0.010	0.9697 ± 0.007	0.9306 ± 0.030	0.9697 ± 0.007	0.9561 ± 0.022
JSC	0.9152 ± 0.024	0.9423 ± 0.018	0.9413 ± 0.013	0.8716 ± 0.049	0.9413 ± 0.013	0.9167 ± 0.031
MSD (mm)	1.3762 ± 0.504	1.0625 ± 0.440	1.1591 ± 0.355	1.4804 ± 0.841	1.1591 ± 0.355	1.3149 ± 0.563
HSD (mm)	29.03 ± 6.61	27.74 ± 7.54	30.83 ± 5.24	23.29 ± 8.94	30.83 ± 5.24	27.89 ± 7.50

Lt, left; *Rt*, right

Table 7 Performance of the proposed lung lobe segmentation method according to COPD GOLD stage level

		LtLower	LtUpper	RtLower	RtMiddle	RtUpper	Overall
Normal ($N = 2$)	DSC	0.9542 ± 0.014	0.9711 ± 0.007	0.9425 ± 0.014	0.9411 ± 0.013	0.9676 ± 0.007	0.9553 ± 0.016
	JSC	0.9125 ± 0.025	0.9440 ± 0.013	0.8913 ± 0.026	0.8889 ± 0.028	0.9372 ± 0.014	0.9148 ± 0.029
	MSD (mm)	0.9613 ± 0.120	0.7815 ± 0.108	1.1452 ± 0.079	1.1119 ± 0.142	1.1061 ± 0.116	1.0212 ± 0.167
	HSD (mm)	22.11 ± 2.82	21.99 ± 1.16	19.53 ± 1.22	17.40 ± 1.59	26.95 ± 3.45	21.60 ± 3.76
COPD GOLD stage 1 ($N = 8$)	DSC	0.9464 ± 0.017	0.9623 ± 0.016	0.9594 ± 0.011	0.9359 ± 0.012	0.9683 ± 0.008	0.9544 ± 0.017
	JSC	0.8986 ± 0.031	0.9277 ± 0.029	0.9221 ± 0.020	0.8798 ± 0.021	0.9386 ± 0.014	0.9133 ± 0.031
	MSD (mm)	1.9134 ± 0.802	1.5553 ± 0.754	1.7244 ± 0.780	1.3699 ± 0.314	1.4257 ± 0.658	1.5977 ± 0.680
	HSD (mm)	31.36 ± 8.15	28.60 ± 9.19	29.12 ± 7.15	24.01 ± 7.93	29.54 ± 5.59	28.53 ± 7.70
COPD GOLD stage 2 ($N = 18$)	DSC	0.9560 ± 0.011	0.9716 ± 0.007	0.9529 ± 0.014	0.9339 ± 0.012	0.9681 ± 0.007	0.9565 ± 0.017
	JSC	0.9159 ± 0.021	0.9448 ± 0.013	0.9103 ± 0.026	0.8762 ± 0.022	0.9382 ± 1.233	0.9171 ± 0.031
	MSD (mm)	1.2691 ± 0.323	0.9111 ± 0.210	1.4455 ± 0.287	1.3495 ± 0.457	1.0423 ± 0.147	1.2035 ± 0.357
	HSD (mm)	28.00 ± 7.21	24.94 ± 4.42	29.11 ± 8.01	20.89 ± 6.21	28.61 ± 4.16	26.31 ± 6.79
COPD GOLD stage 3 ($N = 12$)	DSC	0.9612 ± 0.010	0.9732 ± 0.006	0.9556 ± 0.013	0.9205 ± 0.052	0.9735 ± 0.006	0.9568 ± 0.031
	JSC	0.9255 ± 0.018	0.9479 ± 0.012	0.9153 ± 0.024	0.8565 ± 0.083	0.9484 ± 0.012	0.9187 ± 0.052
	MSD (mm)	1.2478 ± 0.225	1.0080 ± 0.149	1.4789 ± 0.256	1.8194 ± 1.392	1.1653 ± 0.251	1.3424 ± 0.691
	HSD (mm)	30.19 ± 3.99	32.34 ± 8.68	28.74 ± 4.16	27.39 ± 12.21	35.68 ± 3.42	30.87 ± 7.67

Conclusion

In this study, we proposed a fully automated lung lobe segmentation method using U-Net. Since U-Net shows a good performance on image segmentation, we customized the U-Net into 3D and optimized it for lung lobe segmentation in 12-bit medical images with memory limitation of current GPU. In addition, we designed an overall process from preprocessing to error correction, which leads the lung lobe segmentation with high accuracy.

Our method was highly effective not only for the normal group but also for the mild COPD group. Furthermore, it performed well in the presence of fake and incomplete fissures as the method did not rely on the information of the lobar fissures. Our method could be used without manual correction, and we markedly improved the execution time compared with that of other image processing–based methods. To address the overfitting problem of typical deep learning methods, we trained our model using two different datasets, which included independent heterogeneous sets with different scanners and reconstruction kernels. We performed an external validation to evaluate the generalizability of our model.

Funding Information This work was supported by the Industrial Strategic technology development program (10072064) funded by the Ministry of Trade Industry and Energy (MI, Korea).

References

1. Doel T, Gavaghan DJ, Grau V: Review of automatic pulmonary lobe segmentation methods from CT. Comput Med Imaging Graph 40:13–29, 2015
2. Jeffery PK: Structural and inflammatory changes in COPD: a comparison with asthma. Thorax 53(2):129–136, 1998
3. Leung AN: Pulmonary tuberculosis: The essentials. Radiology 210(2):307–322, 1999
4. Morgan EJ: Silicosis and tuberculosis. Chest 75(2):202–203, 1979
5. European, R. S., & American Thoracic Society: American Thoracic Society/European Respiratory Society international multidisciplinary consensus classification of the idiopathic interstitial pneumonias. This joint statement of the American Thoracic Society (ATS), and the European Respiratory Society (ERS) was adopted by the ATS board of directors, June 2001 and by the ERS executive committee, June 2001. Am J Respir Crit Care Med 165(2):277, 2002
6. Lassen B, Kuhnigk JM, Friman O, Krass S, Peitgen HO: Automatic segmentation of lung lobes in CT images based on fissures, vessels, and bronchi. In Biomedical imaging: From Nano to macro, 2010 IEEE international symposium on. IEEE, 2010, pp 560–563.
7. Lassen B, Kuhnigk JM, Schmidt M, Krass S, Peitgen HO: Lung and lung lobe segmentation methods at Fraunhofer MEVIS. In: Fourth international workshop on pulmonary image analysis, vol. 18. 2011, pp 185–99
8. Zhang L, Hoffman EA, Reinhardt JM: Atlas-driven lung lobe segmentation in volumetric X-ray CT images. IEEE Trans Med Imaging 25(1):1–16, 2006
9. Pu J, Zheng B, Leader JK, Fuhrman C, Knollmann F, Klym A, Gur D: Pulmonary lobe segmentation in CT examinations using implicit surface fitting. IEEE Trans Med Imaging 28(12):1986–1996, 2009

10. Kuhnigk JM, Hahn H, Hindennach M, Dicken V, Krass S, Peitgen HO: Lung lobe segmentation by anatomy-guided 3D watershed transform. In: Medical Imaging 2003: Image Processing, vol. 5032. International Society for Optics and Photonics, 2003, pp 1482–1491
11. Zhang L, Hoffman EA, Reinhardt JM: Lung lobe segmentation by graph search with 3D shape constraints. In: Medical Imaging 2001: Physiology and Function from Multidimensional Images, vol. 4321. International Society for Optics and Photonics, 2001, pp 204–216
12. Harrison AP, Xu Z, George K, Lu L, Summers RM, Mollura DJ:. Progressive and multi-path holistically nested neural networks for pathological lung segmentation from CT images. In: International conference on medical image computing and computer-assisted intervention. Cham: Springer, 2017, pp 621–629
13. George K, Harrison AP, Jin D, Xu Z, Mollura DJ: Pathological pulmonary lobe segmentation from CT images using progressive holistically nested neural networks and random Walker. In: Deep learning in medical image analysis and multimodal learning for clinical decision support. Cham: Springer, 2017, pp. 195–203
14. Meenakshi S, Manjunath KY, Balasubramanyam V: Morphological variations of the lung fissures and lobes. Indian J Chest Dis Allied Sci 46:179–182, 2004
15. Leader JK, Zheng B, Rogers RM, Sciurba FC, Perez A, Chapman BE, … Gur D: Automated lung segmentation in X-ray computed tomography: Development and evaluation of a heuristic threshold-based scheme 1. Acad Radiol 10(11):1224–1236,2003
16. Duda RO, Hart PE: Use of the Hough transformation to detect lines and curves in pictures. Commun ACM 15(1):11–15, 1972
17. Lee YJ, Lee M, Kim N, Seo JB, Park JY: Automatic left and right lung separation using free-formed surface fitting on volumetric CT. J Digit Imaging 27(4):538–547, 2014
18. D'Errico J: Surface fitting using Gridfit. In: Matlab Central File Exchange. 2006
19. Dillencourt MB, Samet H, Tamminen M: A general approach to connected-component labeling for arbitrary image representations. J ACM (JACM) 39(2):253–280, 1992
20. Çiçek Ö, Abdulkadir A, Lienkamp SS, Brox T, Ronneberger O: 3D U-net: Learning dense volumetric segmentation from sparse annotation. In International conference on medical image computing and computer-assisted intervention. Cham: Springer, 2016, pp 424–432
21. Ronneberger O, Fischer P, Brox T: U-net: Convolutional networks for biomedical image segmentation. In: International conference on medical image computing and computer-assisted intervention. Cham: Springer, 2015, pp 234–241
22. Long J, Shelhamer E, Darrell T: Fully convolutional networks for semantic segmentation. In: Proceedings of the IEEE conference on computer vision and pattern recognition. 2015, pp 3431–3440
23. Sørensen T: A method of establishing groups of equal amplitude in plant sociology based on similarity of species and its application to analyses of the vegetation on Danish commons. Biol Skr 5:1–34, 1948
24. Bae J, Kim N, Lee SM, Seo JB, Kim HC: Thoracic cavity segmentation algorithm using multiorgan extraction and surface fitting in volumetric CT. Med Phys 41(4), 2014
25. Gallagher E: COMPAH documentation. 1999. User's Guide and application published at: http://www.es.umb.edu/edgwebp.htm
26. Rockafellar RT, Wets RJB: Variational analysis. Springer-Verlag, 2005, p 117. ISBN 3-540-62772-3
27. Pauwels RA, Buist AS, Calverley PM, Jenkins CR, Hurd SS: Global strategy for the diagnosis, management, and prevention of chronic obstructive pulmonary disease: NHLBI/WHO global initiative for chronic obstructive lung disease (GOLD) workshop summary. Am J Respir Crit Care Med 163(5):1256–1276, 2001